

NON-LORENTZIAN SPECTRAL LINESHAPES NEAR A HOPF BIFURCATION*

J. P. GLEESON† AND F. O'DOHERTY†

Abstract. The effects of additive white noise upon the dynamics of a system described by its Hopf normal form are investigated, with particular reference to the well-known model of a detuned single-mode laser. The power spectrum corresponding to the laser amplitude is determined by finite-difference solution of a partial differential equation, and analytical formulas are determined in the asymptotic limits of large parameters. The effect of the amplitude-phase coupling parameter in generating non-Lorentzian lineshapes is highlighted, and the regions of parameter space where accurate first-eigenvalue approximations of the Fokker–Planck equation exist are indicated.

Key words. white noise, stochastic differential equations, Hopf normal form, Fokker–Planck equation, semiconductor lasers, oscillators

AMS subject classifications. 70K45, 82C31, 37N20, 60H40

DOI. 10.1137/040615146

1. Introduction. In this paper we consider the effects of white noise upon the dynamics of a system near a Hopf bifurcation point. The well-known deterministic (noise-free) Hopf normal form is [1]

$$(1) \quad \frac{dE}{dt} = i\Omega E + (1 + i\delta) (a - |E|^2) E,$$

where $E(t)$ is a complex-valued function of time representing, for example, the electric field of a single-mode laser in a semiclassical approximation [2] with fundamental frequency Ω . The parameters a and δ are real-valued and dimensionless; see the Appendix for details of their derivation from the standard normal form parameters. This equation can be written in amplitude-phase coordinates using $E = r \exp(i\theta)$, with the dynamics of the polar coordinates $r(t)$ and $\theta(t)$ being governed by the pair of equations

$$(2) \quad \begin{aligned} \frac{dr}{dt} &= (a - r^2) r, \\ \frac{d\theta}{dt} &= \Omega + \delta (a - r^2). \end{aligned}$$

As discussed in Chapter 12 of [2], noise effects may be incorporated into the deterministic system by the addition of a complex Langevin fluctuation term

$$(3) \quad \Gamma(t) = \xi_x(t) + i \xi_y(t)$$

to the right-hand side of (1). The zero-mean, real-valued white noise processes $\xi_x(t)$ and $\xi_y(t)$ are described by their delta-function autocorrelation functions [2]:

$$(4) \quad \langle \xi_x(t) \xi_x(t') \rangle = \langle \xi_y(t) \xi_y(t') \rangle = 2\delta(t - t'), \quad \langle \xi_x(t) \xi_y(t') \rangle = 0.$$

*Received by the editors September 15, 2004; accepted for publication (in revised form) February 7, 2006; published electronically July 17, 2006. This work was supported by a Science Foundation Ireland Investigator Award to the first author, program 02/IN.1/IM062.

<http://www.siam.org/journals/siap/66-5/61514.html>

†Applied Mathematics, University College Cork, Cork, Ireland (j.gleeson@ucc.ie, fergal1979@hotmail.com).

Note that the noise intensity is set to unity by our choice of length and time units (see the Appendix for details). Angle brackets are used throughout this paper to denote averaging over an ensemble, i.e., taking an expectation value. Our goal is to describe the effects of the noise terms upon the dynamics of the system (2).

Any system undergoing a Hopf bifurcation may be written in the Hopf normal form (1). The deterministic dynamics of the Hopf bifurcation are well understood. When the bifurcation parameter a is negative, the origin $r = 0$ is an attracting point for all trajectories of the system (2) in the absence of noise. As the bifurcation parameter passes through zero and becomes positive, the origin becomes unstable and trajectories are attracted to the stable limit cycle at $r = \sqrt{a}$. The flow on the limit cycle is purely circular, with angular speed Ω . The parameter δ does not affect these steady-state results, but it has important consequences when the system is subject to fluctuations. For example, in the stable limit cycle case $a > 0$, trajectories which are kicked off the limit cycle eventually flow back onto it, moving at an angular speed which varies with their amplitude when $\delta \neq 0$ and being equal to the steady-state speed Ω only when on the limit cycle. Because δ quantifies this effect of amplitude fluctuations upon the phase angle θ , it is sometimes referred to as the *amplitude-phase coupling parameter*. When $a < 0$ the flow into the attracting origin has a spiral structure. Nonzero δ alters the angular speed of the spiral motion and induces a differential rotation effect; i.e., trajectories further from the origin spiral inwards at rates different from those closer to $r = 0$.

In this paper we study the effect of noise on the dynamics of (2), with particular reference to the *correlation function* of E ,¹

$$(5) \quad R(\tau) = \langle E(t)E^*(t + \tau) \rangle,$$

or to its *power spectrum*, which is found by Fourier transforming $R(\tau)$. The deterministic limit cycle solution described above in the case $a > 0$ is periodic, and so the power spectrum of E exhibits a delta-function spike at the frequency Ω . The effect of small random fluctuations modeled by the noise terms ξ_x and ξ_y in (3) is to broaden the peak in the power spectrum, and so generate a finite linewidth. For $a < 0$ the stable solution is $r = 0$, but “precursor” peaks in the power spectrum of E can be seen: these grow in intensity as the bifurcation parameter a is increased towards the bifurcation point [3, 4, 5]. The stable oscillation generated when $a > 0$ is generic and has been studied in many fields, including electric and electronic engineering, chemical physics, and laser physics. As the system (2) has been extensively studied in the laser literature (at least for the case $\delta = 0$), for convenience we will adopt the nomenclature and notation specific to that field. However, our results are applicable to any system of the form (2) in the presence of additive white noise. Recent examples where nonzero values of the parameter δ are important arise in applications to electronic oscillator circuits [5, 6, 7] and to chemical reaction systems [8]. For instance, Coram [7], as a test case for various recently proposed methods [5, 9] for predicting the spectral lineshape of noisy electronic oscillator circuits, proposes a model which (in the limit of small noise) is essentially equivalent to (2). The important new effects due to the amplitude-phase coupling parameter δ demonstrated in this paper are thus also immediately applicable to electronic oscillator models such as Coram’s.

In the laser literature the parameter a is commonly referred to as the *pump parameter*, with the regime $a < 0$ termed *below (lasing) threshold*, and $a > 0$ *above*

¹In the laser physics literature the function $R(\tau)$ is known as the amplitude correlation function; here star denotes complex conjugation.

threshold. The parameter δ has received comparatively little attention in the literature, owing to its relative insignificance in the most commonly studied laser systems. Depending on the physical causes of the effect, the parameter has variously been named the *detuning parameter* [2], the *linewidth enhancement factor* [10], or as noted above, the *amplitude-phase coupling parameter*. The effect of δ is known to be non-negligible in semiconductor lasers, and so we believe this study of its effects is timely. As mentioned above, the Hopf normal form (2) is frequently used as the simplest model of a noisy, self-sustained oscillator in many other fields, e.g., electronic circuit design [7] and chemical reaction dynamics [8], and so a complete description of the power spectrum beyond the well-studied $\delta = 0$ case is of some importance.

The dynamics of Hopf bifurcations with additive noise, but with $\delta = 0$, have been studied by several authors. For instance, Baras, Mansour, and Van den Broek [11] discuss in detail the stationary probability density near a Hopf bifurcation point in the weak noise limit. In the review paper [12] the more general stationary distribution problem for a noisy Hopf bifurcation with a noncircular limit cycle is discussed. The effects of multiplicative [13, 14] or colored noises [15, 16] near a Hopf bifurcation have also been considered, as well as noisy bifurcations in delay-differential equations [17]. Our work concentrates on the simplest additive white noise case, and is new in two respects: first, it describes the spectral lineshape (not just the stationary probability density) of the dynamical system near the bifurcation point, and, second, to our knowledge, this is the first comprehensive study of the important effects of the amplitude-phase coupling parameter δ —most previous studies assume δ to be zero or negligibly small. While we use standard results for the stationary probability density near the bifurcation point (e.g., see (8) below), the focus of our work is on the dynamical effect of δ , as evidenced by the shape of the power spectrum. The distinction is crucial—the stationary probability density is independent of δ , while the spectral lineshape is very sensitive to nonzero δ values.

The most complete study of the δ -effect to date appears to be that of Seybold and Risken [18], referred to hereafter as SR. They approach the Fokker–Planck equation corresponding to (2) using the same methods that were successful in the $\delta = 0$ case [2], i.e., an eigenfunction expansion of the transition probability density. The resulting correlation function is then an infinite sum of exponentials, yielding a power spectrum composed of a sum of Lorentzians. Although the calculation of eigenvalues must be done numerically, a crucial result of SR is that for $\delta < 1.2$ the first term in the infinite series is dominant, and so only this first eigenvalue term need be used to find the spectrum to a high order of accuracy. As shown in Figure 1, this single-Lorentzian expression for the spectrum is accurate to power levels many orders of magnitude below the peak. The divergence between the exact spectrum and the SR approximation seen at high frequencies in Figure 2 can be traced to the inaccuracies in the small-time expansion of the correlation function, as noted in SR. However, near the peak of the spectrum (within, say, three orders of magnitude in power level) the SR Lorentzian form of the spectrum is very accurate for $\delta \lesssim 1$. Thus the description of the spectral lineshape (and linewidth) is reduced to finding the appropriate eigenvalue of the Fokker–Planck equation. We note in passing that this first-eigenvalue approach is also used in recent papers attempting to predict the spectral lineshape arising from noise in electronic oscillator circuits [5, 6] and limit cycles modeling chemical clocks [8].

The SR paper covers only the case $\delta < 1.2$, which encompassed the values of the parameter δ of interest to the laser community at the time. However, more recent research in the field of semiconductor lasers indicates that the values of δ

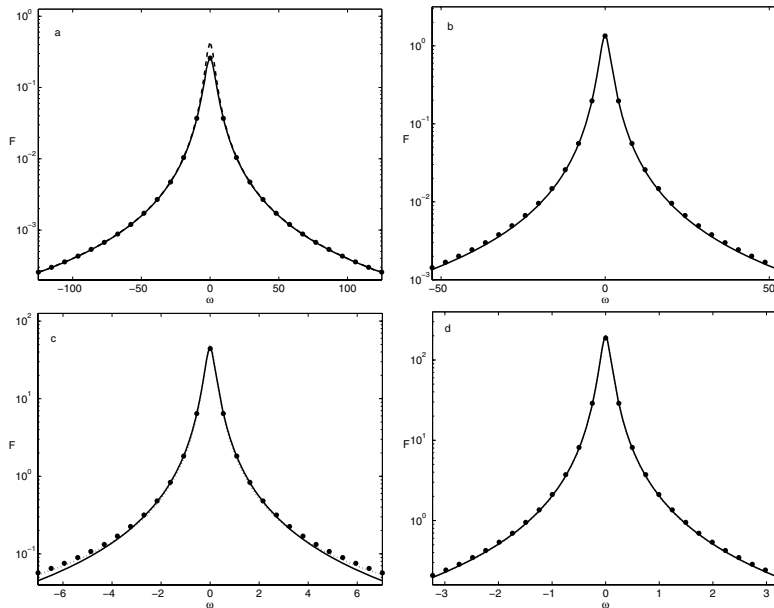


FIG. 1. Spectrum $F(\omega)$ for $\delta = 0$ and various values of a : (a) $a = -3$, (b) $a = 0$, (c) $a = 5$, (d) $a = 10$. Results from the numerical solution (25) are shown as symbols; the solid line is the Lorentzian lineshape (31); the dashed (for $a < 0$) and dotted (for $a > 0$) lines show the asymptotic results of section 4.

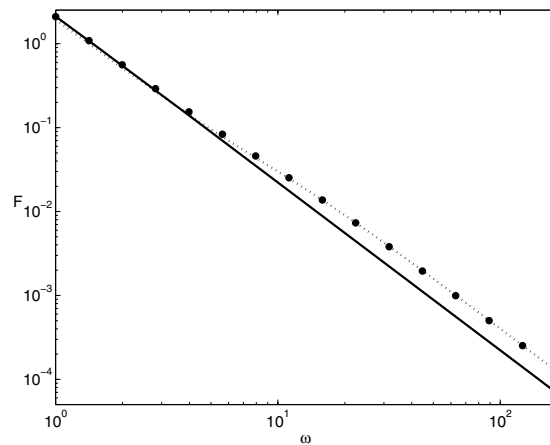


FIG. 2. Log-log plot of the spectrum $F(\omega)$ for large frequencies, with parameters $a = 5$ and $\delta = 0$ (cf. Figure 1(c)). Line types are as in Figure 1.

appropriate to the model (2) are on the order of 5 to 7. The most obvious effect of this larger δ is a significant widening of the spectral line—hence the title of *linewidth enhancement factor* (or simply α -factor) which is sometimes applied to δ . Implicit in most discussions of the linewidth of semiconductor lasers is the belief that the lineshape is intrinsically Lorentzian. Indeed some workers have followed the methods of SR to calculate the first eigenvalue in the case $\delta \geq 5$, and to compare the resulting linewidth to experimental calculations [19]. However, our results, using numerical

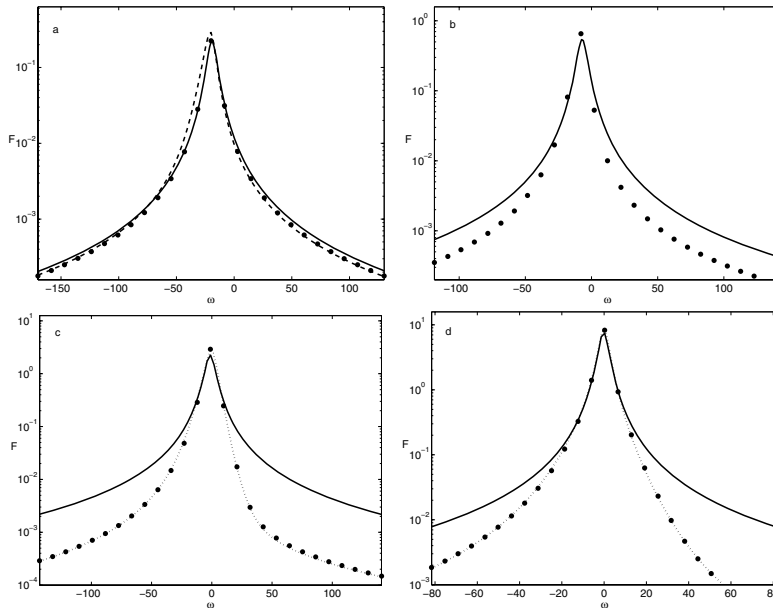


FIG. 3. Spectrum $F(\omega)$ for $\delta = 5$ and various values of a : (a) $a = -3$, (b) $a = 0$, (c) $a = 5$, (d) $a = 10$. See Figure 1 for description of line types.

solutions and asymptotic analysis of the Fokker–Planck equation (see Figures 3 and 4), indicate that the lineshape is markedly non-Lorentzian at $\delta = 5$ (at least for certain values of the pump parameter a). It is therefore useful to experimentalists working with δ levels higher than those examined in SR to have numerical methods and closed form asymptotic solutions which are valid for arbitrarily large values of the parameter δ .

The main results of this paper are presented in caricature form in Figure 5, showing the (a, δ) parameter plane. Since the spectrum for negative δ can be found from the corresponding positive δ result by changing the sign of frequencies ($\omega \rightarrow -\omega$, $\Omega \rightarrow -\Omega$), we consider only $\delta \geq 0$. The hatched region is where the SR first-eigenvalue Lorentzian lineshape fits reasonably well² to the exact spectrum, which we determine by a finite-difference numerical solution of (23) below. As originally shown in SR, the Lorentzian lineshape fits well for all values of the pumping parameter a , provided that δ is less than approximately unity. When δ is significantly greater than one, SR remains accurate very far from the threshold at $a = 0$, but the required magnitude of the pumping increases as δ increases. For instance, we show that for $a < 0$ the SR solution is accurate when the ratio $\delta/a^2 \ll 1$; the corresponding requirement for positive pumping parameter is that $\delta/a \ll 1$. These constraints on the SR solution give the borders of the hatched region above $\delta = 1$. These limits on the single-Lorentzian form of the spectrum are derived using new asymptotic solutions, valid for $|a| \gg 1$ and for all δ values. Our new asymptotic solutions are found to be accurate outside of the region of the (a, δ) plane enclosed by the dashed lines at $a = -5$ and $a = 3$, and show that non-Lorentzian lineshapes are increasingly

²The precise meaning of “reasonably well” of course depends on the level of accuracy desired; Figure 5 is intended to indicate only the estimated (order of magnitude) borders where various approximations hold.

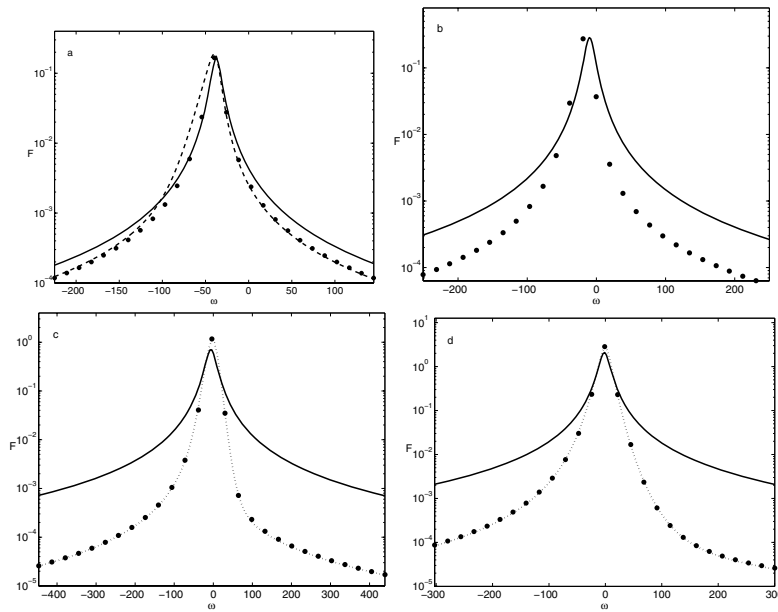


FIG. 4. Spectrum $F(\omega)$ for $\delta = 10$ and various values of a : (a) $a = -3$, (b) $a = 0$, (c) $a = 5$, (d) $a = 10$. See Figure 1 for description of line types.

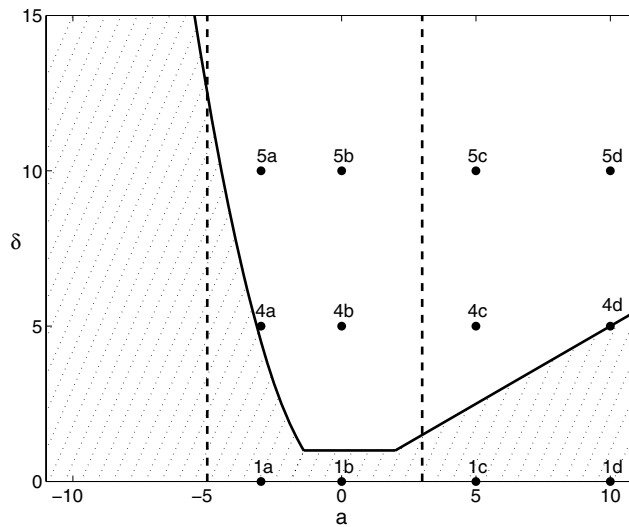


FIG. 5. The (a, δ) parameter plane. The shaded region shows where the single-Lorentzian spectrum of SR matches the exact result reasonably well; the boundaries are taken to be $\delta/a^2 = 1/2$ for $a < 0$, and $\delta/a = 1/2$ for $a > 0$. The new asymptotic results derived in section 4 match the exact results well when $a \ll -5$ or $a \gg 3$. These limits are shown as dashed lines in the figure—note the considerable regions of the parameter plane (e.g., for $a \gg 3$ and $\delta \gg a/2$) where our asymptotic results match the exact values, but those of SR do not. The labeled dots mark the parameter values where spectra are plotted in the corresponding figures.

important as δ increases. The analytical expressions are likely to be useful not only to experimentalists characterizing lineshapes with $\delta > 1$, but also in providing a novel test case for schemes attempting to characterize spectral lineshapes in self-sustained oscillators of arbitrary dimension in various applications [5, 20].

2. Fokker–Planck equation. The dynamics of the system (1) in the presence of the noise term (3) is fully described by the solution of the Fokker–Planck equation [2], which gives the transition probability density $P(\mathbf{x}, \tau|\mathbf{x}', 0)$ of the two-dimensional stochastic process $\mathbf{x}(t)$, written in polar coordinates as $\mathbf{x}(t) = (r(t) \cos \theta(t), r(t) \sin \theta(t))$ using (2). The transition probability density is the probability that a trajectory of the system passes through the point \mathbf{x} at time $t = \tau$, given that it passed through \mathbf{x}' at time $t = 0$. The Fokker–Planck equation is a partial differential equation for P :

$$(6) \quad \frac{\partial P}{\partial \tau} + \frac{1}{r} \frac{\partial}{\partial r} [(a - r^2) r^2 P] + \frac{\partial}{\partial \theta} [(\Omega + \delta (a - r^2)) P] - \frac{1}{r} \frac{\partial}{\partial r} \left[r \frac{\partial P}{\partial r} \right] - \frac{1}{r^2} \frac{\partial^2 P}{\partial \theta^2} = 0,$$

with initial condition

$$(7) \quad P(\mathbf{x}, 0|\mathbf{x}', 0) = \delta(\mathbf{x} - \mathbf{x}'),$$

where here $\delta(\mathbf{x})$ is the Dirac delta-function (not to be confused with the parameter δ , as should be clear from the context). Equation (6) has a stationary ($\tau \rightarrow \infty$) solution which depends only on r (and is independent of δ), as shown in [11, 2]:

$$(8) \quad P_\infty(r) = C \exp\left(\frac{ar^2}{2} - \frac{r^4}{4}\right).$$

The normalization constant C is given in terms of the error function as

$$(9) \quad C = \frac{\exp\left(-\frac{a^2}{4}\right)}{\pi^{\frac{3}{2}} \left[1 + \operatorname{erf}\left(\frac{a}{2}\right)\right]},$$

in order to ensure unit probability over the two-dimensional space

$$(10) \quad \int_0^{2\pi} \int_0^\infty P_\infty(r) r dr d\theta = 1.$$

Note that stationary moments may be calculated from $P_\infty(r)$, for example [2]:

$$(11) \quad \langle r^2 \rangle = a + 2\pi C.$$

The transition probability density may be used to calculate the correlation between arbitrary functionals $f(\mathbf{x})$ and $g(\mathbf{x})$ of the dynamical system trajectories at times separated by τ [2, 21]:

$$(12) \quad \langle f(\mathbf{x}(t)) g(\mathbf{x}(t + \tau)) \rangle = \int d\mathbf{x}' P_\infty(\mathbf{x}') f(\mathbf{x}') \int d\mathbf{x} P(\mathbf{x}, \tau|\mathbf{x}', 0) g(\mathbf{x}),$$

where each of the integrals above is over the two-dimensional trajectory space. The correlation function may be directly related to the Fokker–Planck equation by defining an auxiliary function $Q(\mathbf{x}, \tau)$ as

$$(13) \quad Q(\mathbf{x}, \tau) = \int P_\infty(\mathbf{x}') f(\mathbf{x}') P(\mathbf{x}, \tau|\mathbf{x}', 0) d\mathbf{x}'.$$

Note that this auxiliary function is a solution of the Fokker–Planck differential equation (6):

$$(14) \quad \frac{\partial Q}{\partial \tau} + \frac{1}{r} \frac{\partial}{\partial r} [(a - r^2) r^2 Q] + \frac{\partial}{\partial \theta} [(\Omega + \delta (a - r^2)) Q] - \frac{1}{r} \frac{\partial}{\partial r} \left[r \frac{\partial Q}{\partial r} \right] - \frac{1}{r^2} \frac{\partial^2 Q}{\partial \theta^2} = 0,$$

but with an initial condition that differs from (7):

$$(15) \quad Q(\mathbf{x}, 0) = f(\mathbf{x}) P_\infty(\mathbf{x}).$$

Assuming that the auxiliary function has been determined, the correlation function is then obtained by integration:

$$(16) \quad \langle f(\mathbf{x}(t)) g(\mathbf{x}(t + \tau)) \rangle = \int g(\mathbf{x}) Q(\mathbf{x}, \tau) d\mathbf{x}.$$

The correlation function of the complex quantity E defined in (5) may be calculated by applying this general method, using the functionals

$$(17) \quad f(\mathbf{x}) = r \exp(i\theta) \quad \text{and} \quad g(\mathbf{x}) = r \exp(-i\theta)$$

and the stationary probability density given by (8) and (9). In this case, the auxiliary function is defined as the solution of (14) with initial condition

$$(18) \quad Q(r, \theta, 0) = r e^{i\theta} P_\infty(r),$$

and the desired correlation function is found from Q by integration:

$$(19) \quad R(\tau) = \langle E(t) E^*(t + \tau) \rangle = \int_0^{2\pi} \int_0^\infty r^2 e^{-i\theta} Q(r, \theta, \tau) dr d\theta.$$

The power spectrum of E is defined using the Fourier transform of the correlation function, following the convention of SR:

$$(20) \quad F(\omega) \equiv 2 \operatorname{Re} \left[\int_0^\infty e^{i\omega\tau} R(\tau) d\tau \right].$$

This formulation of the problem in terms of the auxiliary function Q proves extremely useful for both numerical calculations and asymptotic analysis, and thus forms the theoretical basis for the remainder of the paper. While the formulation (12) for correlation functions is common [2, 21], the reduction to a partial differential equation (pde) for an auxiliary function Q is a nonstandard approach. This idea is potentially very useful for the calculation of correlation functions and spectra in low-dimensional systems, where standard numerical methods for pdes may be applied, as in (23) below.

3. Numerical calculations. In this section we compare two methods for numerical calculation of the spectrum. The auxiliary function approach presented in section 3.1 provides the high-accuracy solutions used throughout the paper; the single-eigenvalue spectrum used by Seybold and Risken is also reviewed in section 3.2.

3.1. Auxiliary function approach. The solution of the pde (14) for the auxiliary function is facilitated by noting that the initial condition (18) permits a separable form:

$$(21) \quad Q(r, \theta, \tau) = e^{i\theta} q(r, \tau).$$

Moreover, the power spectrum $F(\omega)$ may be calculated without first finding the correlation function. To see this, multiply (14) by $\exp(i\omega\tau)$ and integrate over τ . The resulting equation for the quantity $\hat{q}(r, \omega)$, defined as

$$(22) \quad \begin{aligned} \hat{q}(r, \omega) &\equiv \int_0^\infty e^{i\omega\tau} q(r, \tau) d\tau \\ &= \int_0^\infty e^{i\omega\tau} e^{-i\theta} Q(r, \theta, \tau) d\tau, \end{aligned}$$

is an ordinary differential equation, parameterized by the frequency ω :

$$(23) \quad -i\omega\hat{q} - rP_\infty(r) + \frac{1}{r} \frac{d}{dr} [(a - r^2) r^2 \hat{q}] + i\Omega\hat{q} + i\delta (a - r^2) \hat{q} - \frac{1}{r} \frac{d}{dr} \left[r \frac{d\hat{q}}{dr} \right] + \frac{1}{r^2} \hat{q} = 0.$$

The boundary conditions on \hat{q} are

$$(24) \quad \begin{aligned} \hat{q} &\rightarrow 0 \quad \text{as } r \rightarrow 0, \\ \hat{q} &\rightarrow 0 \quad \text{as } r \rightarrow \infty. \end{aligned}$$

Equation (23) is solved numerically for each frequency ω using a standard finite-difference algorithm. The boundary condition for $r \rightarrow \infty$ is implemented by truncating the finite-difference grid at a large value of r and setting a Dirichlet condition at the truncation point. We check that this truncation point is sufficiently large to have negligible effect on all spectra shown. Finally, the spectrum $F(\omega)$ is calculated directly from \hat{q} by numerical integration:

$$(25) \quad F(\omega) = 4\pi \operatorname{Re} \left[\int_0^\infty r^2 \hat{q}(r, \omega) dr \right].$$

The accuracy of the finite-difference solution depends only on the number of grid points and on the truncation point, and so effectively gives an exact solution for the spectrum. The values found from this numerical method are plotted as symbols in the figures and enable us to compare various analytical approximations for the spectrum.

3.2. Eigenfunction expansion. The formulation given in SR (see also [2]) uses (12) to calculate the correlation function, but instead of defining the auxiliary function and solving (14), the Fokker–Planck equation (6) for the transition probability density $P(\mathbf{x}, \tau | \mathbf{x}', 0)$ is solved directly. The solution may be found by an eigenfunction expansion [18] or by expansion into a complete set as in [2], i.e., writing P as

$$(26) \quad P(r, \theta, \tau | r', \theta', 0) = \frac{1}{2\pi} e^{-r^2/\alpha} \sum_{n=0}^\infty \sum_{\nu=-\infty}^\infty c_n^{(\nu)} \left(\frac{r'^2}{\alpha}, \tau \right) r^{|\nu|} \alpha^{-|\nu|/2} L_n^{(|\nu|)} \left(\frac{r^2}{\alpha} \right) e^{i\nu(\theta-\theta')}.$$

Here $L_n^{(|\nu|)}$ denotes the generalized Laguerre function, and α is a scaling parameter which can be varied to improve the accuracy of a truncated series approximation

to (26). The coefficients $c_n^{(\nu)}$ satisfy ordinary differential equations, which may be written as

$$(27) \quad \frac{dc_n^{(\nu)}}{d\tau} = \sum_{m=0}^{\infty} A_{nm}^{(\nu)} c_m^{(\nu)},$$

with initial conditions derived from (7); see [2] for details. To solve numerically, we truncate the sums over n and m in (26) and (27) at a large integer N , and for each ν solve for $c_n^{(\nu)}$ using the matrix exponential of the $(N+1) \times (N+1)$ complex-valued matrix $\mathbf{A}^{(\nu)}\tau$. The final result for the correlation function (19) is then of the form

$$(28) \quad R_{SR}(\tau) = \langle r^2 \rangle \sum_{n=0}^N V_n e^{\Lambda_n \tau},$$

where Λ_n are the eigenvalues of the matrix $\mathbf{A}^{(1)}$, and the V_n depend upon the eigenvectors and the initial conditions. The value of $\langle r^2 \rangle$ is given in (11). All Λ_n have negative real parts, so the dominant term when the separation time τ is large gives

$$(29) \quad R_{SR}(\tau) \sim \langle r^2 \rangle V_0 e^{\Lambda_0 \tau} \quad \text{as } \tau \rightarrow \infty,$$

where Λ_0 is the eigenvalue of $\mathbf{A}^{(1)}$ with largest real part. The corresponding spectrum is

$$(30) \quad F_{SR}(\omega) = 2 \langle r^2 \rangle \operatorname{Re} \left[\frac{V_0}{-\Lambda_0 - i\omega} \right].$$

Seybold and Risken [18] take $V_0 \equiv 1$ (with error of less than 3% when $\delta \leq 1.2$), and we therefore compare our numerical results to the SR first-eigenvalue spectrum

$$(31) \quad F_{SR} = 2 \langle r^2 \rangle \frac{|\Lambda_{0r}|}{\Lambda_{0r}^2 + (\Lambda_{0i} + \omega)^2},$$

with Λ_{0r} and Λ_{0i} being the real and imaginary parts of Λ_0 . This Lorentzian spectrum is peaked at frequency $\omega = \omega_p = -\Lambda_{0i}$ and reaches half of its peak power at frequencies $\omega = \omega_p \pm \Delta\omega$, where $\Delta\omega = |\Lambda_{0r}|$. The frequency difference $\Delta\omega$ gives the half-width of the Lorentzian spectrum at half of the peak value, and when normalized by $\langle r^2 \rangle$ it is referred to as the half-width-at-half-maximum (HWHM), or simply *linewidth*, of the laser spectral line. The spectrum (31) is plotted as a solid line in the figures for comparison with numerical values calculated using the auxiliary function method (symbols), and with asymptotic approximations. The linewidth is examined further in Figures 6 and 7, see section 4.1.

4. Asymptotic solutions. To simplify our notation and conform with the usual conventions in the laser physics literature [18], we set the fundamental frequency Ω to zero in (2). Note that this can formally be accomplished by moving to a rotating reference frame, i.e., changing the angular variable from θ to $\theta - \Omega t$. This change of frame shifts the spectrum so that the peak at $\omega = \Omega$ in the original frame is moved to $\omega = 0$. All results reported here are thus at frequencies ω relative to the fundamental frequency Ω .

4.1. Above threshold: $a \gg 1$. The deterministic dynamics of (2) for positive values of the pump parameter a lead to limit cycles of radius \sqrt{a} , as discussed in section 1. When a is sufficiently large, the effects of the (order one) noise terms on the amplitude are small compared to \sqrt{a} . The behavior of the dynamics close to the deterministic limit cycle may be examined by making the change of variables

$$(32) \quad r = \sqrt{a} + \frac{\rho}{\sqrt{2a}}$$

in (14). This scaling focuses close to the limit cycle at $r = \sqrt{a}$, with (as shown below) the new variable ρ being of order one in the region of interest. The variable ρ is interpreted as a linear variable, with range $(-\infty, \infty)$ in the $a \rightarrow \infty$ limit. The two-dimensional area integral is modified as follows:

$$(33) \quad \int_0^{2\pi} \int_0^\infty r \, dr \, d\theta \longrightarrow \frac{1}{\sqrt{2}} \int_0^{2\pi} \int_{-\infty}^\infty d\rho \, d\theta,$$

and the stationary probability density becomes

$$(34) \quad P_\infty(\rho) = \frac{1}{2\pi^{3/2}} \exp\left(-\frac{\rho^2}{2}\right).$$

Using (32) in (14) leads to the linearized equation

$$(35) \quad \frac{\partial Q}{\partial \tau} - 2a \frac{\partial}{\partial \rho} (\rho Q) - \sqrt{2}\delta\rho \frac{\partial Q}{\partial \theta} - 2a \frac{\partial^2 Q}{\partial \rho^2} - \frac{1}{a} \frac{\partial^2 Q}{\partial \theta^2} = 0,$$

where the first term of an asymptotic expansion for $a \rightarrow \infty$ replaces each term in (14). The initial condition (18) is expanded to

$$(36) \quad Q(\tau = 0) = \sqrt{a} \left(1 + \frac{\rho}{\sqrt{2a}}\right) e^{i\theta} P_\infty(\rho).$$

Equation (35) with initial condition (36) may be solved exactly by Fourier transforming in ρ and using the method of characteristics [2]. Separating variables as in (21) and defining the spatial Fourier transform as

$$(37) \quad \tilde{q}(k, \tau) = \int_{-\infty}^\infty e^{i\rho k} q(\rho, \tau) \, d\rho,$$

we obtain the hyperbolic equation

$$(38) \quad \frac{\partial \tilde{q}}{\partial \tau} + (2ak - \sqrt{2}\delta) \frac{\partial \tilde{q}}{\partial k} = -\left(2ak^2 + \frac{1}{a}\right) \tilde{q}$$

with initial condition

$$(39) \quad \tilde{q}(k, 0) = \frac{1}{\pi} \sqrt{\frac{a}{2}} \left(1 + i \frac{k}{\sqrt{2a}}\right) e^{-\frac{1}{2}k^2}.$$

Solving (38) by the method of characteristics leads to the solution

$$(40) \quad \tilde{q}(k, \tau) = \frac{1}{\pi} \sqrt{\frac{a}{2}} [f_1(\tau) + f_2(\tau)k] \exp\left[-\frac{1}{2}k^2 + f_3(\tau)k - D(\tau)\right],$$

where

$$\begin{aligned}
 f_1(\tau) &= 1 + i \frac{\delta}{2a^2} (1 - e^{-2a\tau}), \\
 f_2(\tau) &= i \frac{1}{\sqrt{2}a} e^{-2a\tau}, \\
 f_3(\tau) &= \frac{\delta}{\sqrt{2}a} (e^{-2a\tau} - 1), \\
 (41) \quad D(\tau) &= \frac{1}{a}\tau + \frac{\delta^2}{2a^2} (2a\tau + e^{-2a\tau} - 1).
 \end{aligned}$$

The correlation function (19) can be related directly to the Fourier transform of Q via

$$(42) \quad R(\tau) = \sqrt{2a\pi} \left[\tilde{q} - i \frac{1}{\sqrt{2}a} \frac{\partial \tilde{q}}{\partial k} \right] \Big|_{k=0},$$

and the final result may be written as

$$(43) \quad R(\tau) = a (a_0 + a_1 e^{-2a\tau} + a_2 e^{-4a\tau}) e^{-D(\tau)},$$

where the coefficients a_n depend upon the parameters as follows:

$$\begin{aligned}
 a_0 &= \left(1 + \frac{\delta}{2a^2} i \right)^2, \\
 a_1 &= \frac{1}{2a^2} \left(1 + \frac{\delta^2}{a^2} - 2\delta i \right), \\
 (44) \quad a_2 &= -\frac{\delta^2}{4a^4}.
 \end{aligned}$$

Note that for convenience we have assumed $\tau > 0$ in the above; the symmetry of R implies that for negative arguments τ should be replaced by $|\tau|$.

Analytical expressions may be found for the Fourier transform of (43). For instance, a series expansion of the $\exp(D(\tau))$ term allows the autocorrelation to be written as

$$(45) \quad R(\tau) = a \exp\left(\frac{\delta^2}{2a^2}\right) \sum_{n=0}^{\infty} b_n e^{-\lambda_n \tau},$$

with $\lambda_n = 2an + \frac{1}{a}(\delta^2 + 1)$, and

$$(46) \quad b_0 = \left(1 + \frac{\delta^2}{2a^2} i \right)^2,$$

$$(47) \quad b_1 = \frac{1}{2a^2} \left(1 + \frac{\delta^2}{2a^2} - i\delta \right)^2,$$

$$(48) \quad b_n = \frac{(-1)^{n+1} \delta^{2n-2}}{n! 2^n a^{2n}} \left[n + \frac{\delta^2}{2a^2} - i\delta \right]^2 \quad \text{for } n \geq 2.$$

The corresponding spectrum is then an infinite sum of Lorentzians,

$$(49) \quad F(\omega) = 2a \exp\left(\frac{\delta^2}{2a^2}\right) \operatorname{Re} \left[\sum_{n=0}^{\infty} \frac{b_n}{\lambda_n - iw} \right].$$

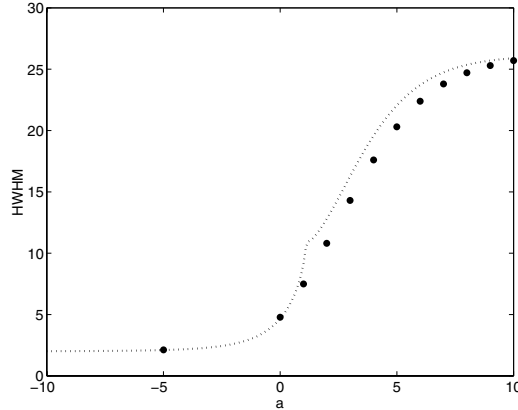


FIG. 6. The normalized linewidth (HWHM) $\langle r^2 \rangle \Delta\omega$ of the spectra as a function of a for $\delta = 5$. Numerical results are shown by symbols; the dotted line is the SR first-eigenvalue result.

Note that this sum converges very slowly when $|\delta| \gg 1$, so that many terms are required to give the spectrum accurately. Also, the leading-order dependence on δ is of the form δ/a ; this implies that non-Lorentzian lineshapes arise when δ is a nonnegligible fraction of a , and leads us to sketch the estimated border $\delta = a/2$ for positive a in Figure 5.

An alternative expression for the spectrum may be given in terms of a finite sum, but involving the generalized incomplete gamma function [22, 23], defined as

$$(50) \quad \gamma(y, z) = \int_0^z t^{y-1} e^{-t} dt.$$

In terms of this function, the spectrum is

$$(51) \quad F(\omega) = \exp\left(\frac{\delta^2}{2a^2}\right) \operatorname{Re} \left[\sum_{n=0}^2 a_n \left(\frac{2a^2}{\delta^2}\right)^{\frac{\lambda_n - i\omega}{2a}} \gamma\left(\frac{\lambda_n - i\omega}{2a}, \frac{\delta^2}{2a^2}\right) \right],$$

with the coefficients a_n as defined in (44). The spectrum (51) is plotted with a dotted line in parts (c) and (d) of Figures 1, 3, and 4, and matches the numerical spectrum (symbols) very well, even for values of a as low as 5. The SR Lorentzian spectrum (solid line) fits poorly when $\delta > 0$. Close to the peak of the spectrum the fit of the SR approximation can be quantified by the HWHM of the lineshape, as defined in section 3.2. The fit of the numerical linewidth to the SR prediction is reasonably good at $\delta = 5$ (Figure 6), indicating that the non-Lorentzian effects have most impact away from the peak; however, the SR linewidth estimation decays in accuracy as δ increases; see the $\delta = 10$ case in Figure 7.

4.1.1. Large-frequency spectrum. A small- τ expansion of $R(\tau)$ from (43) yields

$$(52) \quad R(\tau) \sim a - 2(1 - i\delta)|\tau| + O(\tau^2, a^{-1}) \quad \text{as } \tau \rightarrow 0, a \rightarrow \infty,$$

and the corresponding large-frequency asymptotic form of the spectrum $F(\omega)$ from (20) is

$$(53) \quad F(\omega) \sim \frac{4}{\omega^2} + O(\omega^{-3}) \quad \text{as } \omega \rightarrow \infty.$$

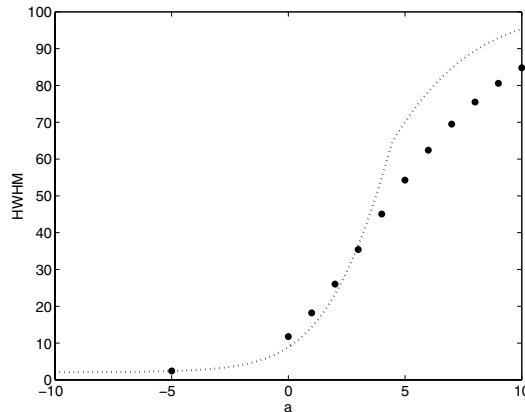


FIG. 7. The normalized linewidth (HWHM) $\langle r^2 \rangle \Delta\omega$ of the spectra as a function of a for $\delta = 10$. Line types are as in Figure 6.

Note that this leading order behavior of the spectrum can be derived directly from a small- τ expansion in (14) and (19), and is independent of the values of the parameters a and δ .

In the $a \gg 1$ asymptotic limit, the single-Lorentzian form of the spectrum used in SR corresponds to the correlation function

$$(54) \quad R_{\text{SR}}(\tau) = a \exp \left[-\frac{1}{a} (1 + \delta^2) |\tau| \right].$$

The large-frequency asymptote of the SR spectrum is then [18]

$$(55) \quad F_{\text{SR}} \sim \frac{2(1 + \delta^2)}{\omega^2} + O(\omega^{-3}) \quad \text{as } \omega \rightarrow \infty$$

and clearly does not match the exact result (53) for general δ . The mismatch of the exact spectrum and the SR approximation far from the peak can be clearly seen in Figure 2. As noted by SR, this effect occurs even when $\delta = 0$. We show in the following sections that the correct large-frequency asymptote depends upon the consistent inclusion of random fluctuations in the amplitude r of the oscillations.

4.1.2. Comparison with other approximations. The above-threshold laser regime has been the subject of many theoretical and experimental investigations. Here we compare our results for $|a| \gg 1$ with other approximation schemes yielding non-Lorentzian lineshapes.

The Langevin equations arising from (2) and (3) may be linearized near the deterministic orbit by the change of variables (32) to give (with $\Omega = 0$)

$$(56) \quad \frac{d\rho}{dt} = -2a\rho + \sqrt{2a}\xi_r,$$

$$(57) \quad \frac{d\theta}{dt} = -\sqrt{2}\delta\rho + \frac{1}{\sqrt{a}}\xi_\theta.$$

Here $\xi_r(t)$ and $\xi_\theta(t)$ are independent, unit intensity white noise terms; cf. the Fokker-Planck equation (35). Equation (56) is linear in ρ with a white-noise forcing, and so

generates an Ornstein–Uhlenbeck colored-noise process $\rho(t)$. Equation (57) describes the stochastic process of the phase angle $\theta(t)$, which is forced by the colored-noise process $\rho(t)$ and the white noise ξ_ρ .

In the full description of the correlation function (5), fluctuations in both the phase $\theta(t)$ and the amplitude $r(t)$ of the oscillation have important effects. The linearized Langevin equations, however, suggest the use of a *phase oscillator* approximation [24], wherein the effects of the colored noise ρ are incorporated into the evolution of the phase angle θ , but all other influence of the amplitude fluctuations are neglected. Under this approximation, the correlation function (5) is simply

$$(58) \quad R_{PO}(\tau) = a \langle \exp [i\theta(t) - i\theta(t + \tau)] \rangle$$

and can be calculated directly from the linearized Langevin equation for θ . The result is [22]

$$(59) \quad R_{PO}(\tau) = a e^{-D(\tau)},$$

where $D(\tau)$ is given in (41). Note that this corresponds to setting $a_0 = 1$ and $a_1 = a_2 = 0$ in the asymptotic result (43).

The spectrum of (59) is non-Lorentzian for $\delta > 0$, but the large-frequency asymptote is

$$(60) \quad F_{PO} \sim \frac{2}{\omega^2} + O(\omega^{-3}) \quad \text{as } \omega \rightarrow \infty,$$

i.e., a factor of 2 lower than the correct form (53). This discrepancy is due to the neglect of the direct effect of amplitude fluctuations upon the spectrum of E within the phase oscillator approximation; the correct values of a_0 , a_1 , and a_2 from (44) are required for the full description of the spectrum.

The *Voigt lineshape*, obtained by convoluting a Lorentzian and a Gaussian in frequency space, is sometimes fitted to experimental oscillation data [25, 26]. We note that in the phase-oscillator approximation the correlation function (59) is the exponential of the function $D(\tau)$; if this function is assumed to be replaced by the first two terms of its Taylor series about $\tau = 0$, the resulting correlation function

$$(61) \quad R_V(\tau) = a e^{-\frac{1}{\alpha}|\tau| - \delta^2 \tau^2}$$

corresponds to a Voigt spectral lineshape. This result can also be derived directly from the linearized phase equation (57) if the amplitude deviation ρ is assumed to be a (frozen) random variable chosen from the Gaussian distribution (34). This approximation completely ignores the temporal variation of $\rho(t)$ as given in (56), and is valid only in the limit $\delta \rightarrow \infty$.

4.2. Below threshold: $a \ll -1$. When the pumping parameter a is negative, the origin $r = 0$ is the attracting steady solution of the deterministic system (2). In order to find asymptotic solutions valid for $a \ll -1$, we therefore rescale lengths to closely examine the neighborhood of the origin:

$$(62) \quad r = \frac{1}{\sqrt{|a|}} \rho,$$

where ρ is of order one and is restricted to the interval $[0, \infty)$. The two-dimensional area integral transforms as

$$(63) \quad \int_0^{2\pi} \int_0^\infty r \, dr \, d\theta \longrightarrow \frac{1}{|a|} \int_0^{2\pi} \int_0^\infty \rho \, d\rho \, d\theta,$$

and the stationary probability density is

$$(64) \quad P_\infty(\rho) = \frac{|a|}{2\pi} \exp\left(-\frac{\rho^2}{2}\right).$$

Retaining the most significant terms (and all δ -dependent terms) in (14) as $|a| \rightarrow \infty$ yields the asymptotic equation

$$(65) \quad \frac{\partial Q}{\partial \tau} + \frac{a}{\rho} \frac{\partial}{\partial \rho} (\rho^2 Q) + \left(a\delta + \frac{1}{a}\delta\rho^2\right) \frac{\partial Q}{\partial \theta} + \frac{a}{\rho} \frac{\partial}{\partial \rho} \left(\rho \frac{\partial Q}{\partial \rho}\right) + \frac{a}{\rho^2} \frac{\partial^2 Q}{\partial \theta^2} = 0,$$

with initial condition

$$(66) \quad Q(\tau = 0) = \frac{\sqrt{|a|}}{2\pi} e^{i\theta} \rho e^{-\frac{1}{2}\rho^2}.$$

Motivated by work in the mixing of scalar fields in vortex fluid flows [27, 28], we seek a solution of (65) in the form

$$(67) \quad Q = \frac{\sqrt{|a|}}{2\pi} e^{i\theta} \rho \exp[-g(\tau)\rho^2 + h(\tau)].$$

This is an *exact* solution of the equation if g and h satisfy the ordinary differential equations

$$(68) \quad \begin{aligned} \frac{1}{|a|} \frac{dg}{d\tau} &= 2g - 4g^2 - i\frac{\delta}{a^2}, \\ \frac{1}{|a|} \frac{dh}{d\tau} &= -8g + 3 + i\delta, \end{aligned}$$

with initial conditions $g(0) = 1/2$, $h(0) = 0$. The solutions of this system may be obtained in closed form, and the correlation function resulting from the integration (19) is

$$(69) \quad \begin{aligned} R(\tau) &= \frac{1}{|a|} \int_0^\infty \rho^3 \exp[-g(\tau)\rho^2 + h(\tau)] d\rho \\ &= \frac{1}{2|a|g^2(\tau)} \exp[h(\tau)] \\ &= \frac{2(1-4\mu)^2}{|a|(1-2\mu)^4} \exp[(-1+i\delta+8\mu)|a\tau|] \left\{ 1 - \frac{4\mu^2}{(1-2\mu)^2} \exp[(-2+8\mu)|a\tau|] \right\}^{-2}, \end{aligned}$$

where $\mu = (1 - \sqrt{1 - 4i\delta/a^2})/4$.

In contrast to the above-threshold case in section 4.1, an analytical formula for the spectrum corresponding to this correlation function has not been found. However, numerical integration of (20) using (69) can be used to find the asymptotic spectrum for $a \ll -1$, valid for arbitrarily large values of δ . This spectrum is plotted for $a = -3$ as a dashed line in part (a) of Figures 1, 3, and 4. The requirement $a \ll -1$ for validity of the asymptotics does not really hold at the chosen value of a , and the fit to the numerical spectrum is poor near the peak, though better than the SR lineshape away from the peak. However, for $a = -10$, Figure 8 shows an excellent match between the asymptotic spectrum and the numerics—here we have taken $\delta = 200$ (so that $\delta/a^2 = 2$) in order to highlight the non-Lorentzian lineshape. Note that the non-Lorentzian effects in (69) depend on the parameter combination δ/a^2 ; this leads us to define the border $\delta/a^2 = 1/2$ for negative a in Figure 5.

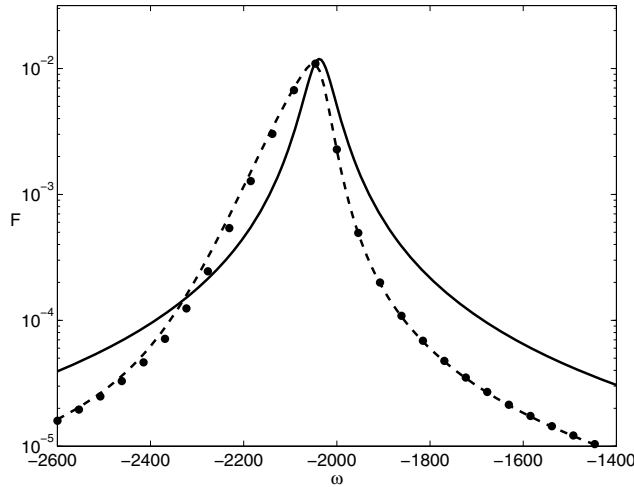


FIG. 8. Spectrum $F(\omega)$ for $a = -10$ and $\delta = 200$. See Figure 1 for description of line types.

5. Conclusions. We have studied the effects of additive white noise on the spectral lineshape of a dynamical system described by the Hopf normal form (1). Particular emphasis is laid on the role of the amplitude-phase coupling (detuning) parameter δ . Non-Lorentzian lineshapes occur when δ is nonnegligible, in contrast to the heretofore most studied case of $\delta = 0$.

We use asymptotic methods to find closed form solutions for the laser amplitude correlation function, valid for any δ value, when the pump parameter a is both above (equation (43)) and below (equation (69)) threshold. In the former case an analytic formula for the spectrum is also given. The asymptotics are formally valid for $|a| \gg 1$, but we find they match the numerical solution well even when the magnitude of a is as small as 5. In contrast to previous work on this problem, no assumption on the size of δ is made, so that the formulas are valid for arbitrarily large δ values. The spectrum becomes non-Lorentzian as δ increases, and we indicate (Figure 5) the parameter regions where single-eigenvalue methods fail to accurately describe the lineshape. We look at existing approximation methods (section 4.1.2) and show that they are special limiting cases of our results.

Both asymptotic and numerical solutions are based on the auxiliary function approach developed in section 2. It should be stressed that (despite the use of convenient nomenclature from the laser physics literature) the results presented are quite general and apply to any noisy dynamical system near a Hopf bifurcation point. We anticipate that the results and methods presented here will be of interest both for their applicability to high- δ lasers, and as test cases for single-eigenvalue methods developed to predict spectra in high-dimensional oscillators for electronic and chemical applications [5, 8, 20]. It would also be interesting to apply the asymptotic methods used here to more detailed models of lasers which supplement (1) with equations for the laser gain and carrier density, leading to relaxation oscillation sidebands in the spectrum [29].

Appendix. The Hopf normal form equations (2) contain only three parameters: a , Ω , and δ . In this appendix we describe in detail the derivation of (2), beginning

with the standard deterministic Hopf normal form presented in [1]:

$$(70) \quad \begin{aligned} \frac{d\tilde{r}}{d\tilde{t}} &= (d\mu + \tilde{a}\tilde{r}^2)\tilde{r}, \\ \frac{d\theta}{d\tilde{t}} &= \omega + c\mu + b\tilde{r}^2. \end{aligned}$$

(Here we use tildes to distinguish between certain parameters and dimensionless versions of the same name.) The parameters \tilde{a} , b , c , and d are all typically of order unity, with $\tilde{a} < 0$, and can in theory be found from the properties of the dynamical system at the bifurcation point $\mu = 0$. The bifurcation parameter is μ , and for analysis “near” the bifurcation point, the magnitude of μ is assumed to be small: $|\mu| \ll 1$. The differential equation for the evolution of the complex quantity $\tilde{E} = \tilde{r} \exp(i\theta)$ follows from (70); the effect of random fluctuations is modeled by adding a white noise term $\tilde{\Gamma}$:

$$(71) \quad \frac{d\tilde{E}}{d\tilde{t}} = i(\omega + c\mu)\tilde{E} + \left(d\mu + (\tilde{a} + ib)|\tilde{E}|^2\right)\tilde{E} + \tilde{\Gamma},$$

with

$$(72) \quad \tilde{\Gamma} = \tilde{\xi}_x(t) + i\tilde{\xi}_y(t)$$

being a complex noise of intensity κ :

$$(73) \quad \langle \tilde{\xi}_x(t)\tilde{\xi}_x(t') \rangle = \langle \tilde{\xi}_y(t)\tilde{\xi}_y(t') \rangle = 2\kappa\delta(t-t'), \quad \langle \tilde{\xi}_x(t)\tilde{\xi}_y(t') \rangle = 0.$$

As further discussed below, the balance between the noise intensity κ and the (small-magnitude) bifurcation parameter μ is crucial to understanding the effects of noise upon the dynamics.

To nondimensionalize the system, we write the Fokker–Planck equation for (71) in the polar coordinates \tilde{r} and θ :

$$(74) \quad \frac{\partial P}{\partial \tilde{\tau}} + \frac{1}{\tilde{r}} \frac{\partial}{\partial \tilde{r}} [(d\mu + \tilde{a}\tilde{r}^2)\tilde{r}^2 P] + \frac{\partial}{\partial \theta} [(\omega + c\mu + b\tilde{r}^2)P] - \frac{\kappa}{\tilde{r}} \frac{\partial}{\partial \tilde{r}} \left[\tilde{r} \frac{\partial P}{\partial \tilde{r}} \right] - \frac{\kappa}{\tilde{r}^2} \frac{\partial^2 P}{\partial \theta^2} = 0.$$

Choosing a length scale L and a time scale T as references, \tilde{r} and $\tilde{\tau}$ may be written in terms of the dimensionless variables r and τ used in (2):

$$(75) \quad \tilde{r} = Lr, \quad \tilde{\tau} = T\tau.$$

The Fokker–Planck equation (74) then becomes

$$(76) \quad \begin{aligned} \frac{\partial P}{\partial \tau} + \frac{1}{r} \frac{\partial}{\partial r} [(Td\mu + TL^2\tilde{a}r^2)r^2 P] + \frac{\partial}{\partial \theta} [(T\omega + Tc\mu + TL^2br^2)P] - \frac{\kappa T}{L^2} \frac{1}{r} \frac{\partial}{\partial r} \left[r \frac{\partial P}{\partial r} \right] \\ - \frac{\kappa T}{L^2} \frac{1}{r^2} \frac{\partial^2 P}{\partial \theta^2} = 0. \end{aligned}$$

We can now choose the length and time scales L and T in order to reduce the number of dimensionless parameters. The conventional choice in the laser literature (see, e.g.,

Chapter 12 of [2]) is to set the diffusion coefficients $\kappa T/L^2$ to unity, and the parameter combination $TL^2\tilde{a}$ to -1 (recall that \tilde{a} is negative). These choices determine T and L in terms of the parameter \tilde{a} and the noise intensity κ , and yield the nondimensional Fokker–Planck equation:

$$(77) \quad \frac{\partial P}{\partial \tau} + \frac{1}{r} \frac{\partial}{\partial r} [(a - r^2) r^2 P] + \frac{\partial}{\partial \theta} [(\Omega + \delta (a - r^2)) P] - \frac{1}{r} \frac{\partial}{\partial r} \left[r \frac{\partial P}{\partial r} \right] - \frac{1}{r^2} \frac{\partial^2 P}{\partial \theta^2} = 0,$$

as used in (6). The parameters a , Ω , and δ appearing here are thus given in terms of the original system parameters as

$$(78) \quad a = d\mu \sqrt{\frac{-1}{\kappa\tilde{a}}}, \quad \Omega = \sqrt{\frac{-1}{\kappa\tilde{a}}} \left(\omega + c\mu - \frac{bd\mu}{\tilde{a}} \right), \quad \delta = \frac{b}{\tilde{a}}.$$

Note the appearance of the bifurcation parameter μ and the noise intensity κ in the definition of the parameter a . As stated above, the magnitude of μ must be small, $|\mu| \ll 1$, for analysis near the Hopf bifurcation point. However, the noise intensity κ may also be very small, and the resulting parameter a may therefore have arbitrarily large magnitude even for small $|\mu|$ if the noise intensity κ goes to zero. Note also that the amplitude-phase coupling parameter δ is independent of μ and depends only on the properties of the dynamical system at the bifurcation point (as determined by the parameters b and \tilde{a} in the normal form (70)).

The derivation of the normal form equations at a bifurcation point relies on the transformation of the dependent and/or independent variables in the original system. The assumption made above that the noise terms enter additively into (71) is therefore somewhat simplistic—when the noise in the original dynamical system is subject to the normal form transformation, it may very well appear in (71) as, for example, multiplicative noise [13], or with unequal intensities in the real and imaginary directions. Nevertheless, the generality of the normal form is such that the study of the simplest case, i.e., additive isotropic white noise, is still instructive. Moreover, additive isotropic noise is often adopted as a phenomenological model when the details of the noise sources or the underlying dynamical system are not known; this is the case for the semiclassical laser equations as derived in Chapter 12 of [2], for example. It is hoped that the new results of this paper (especially on the importance of the amplitude-phase coupling parameter δ) for additive isotropic noise will stimulate further work on the combined effects on spectral lineshapes with nonzero δ and multiplicative and/or nonisotropic noise.

Acknowledgments. The authors gratefully acknowledge helpful discussions with Dr. Guillaume Huyet and Prof. M. P. Kennedy.

REFERENCES

- [1] S. WIGGINS, *Introduction to Applied Nonlinear Dynamical Systems and Chaos*, Springer-Verlag, New York, Berlin, 1989.
- [2] H. RISKEN, *The Fokker–Planck Equation*, 2nd ed., Springer, New York, 1989.
- [3] K. WIESENFELD, *Period doubling bifurcations: What good are they?*, in *Noise in Nonlinear Dynamical Systems*, vol. 2, F. Moss and P. V. E. McClintock, eds., Cambridge University Press, Cambridge, UK, 1989, pp. 145–175.
- [4] K. WIESENFELD, *Noisy precursors of nonlinear instabilities*, *J. Statist. Phys.*, 38 (1985), pp. 1071–1097.

- [5] A. DEMIR, A. MEHROTRA, AND J. ROYCHOWDHURY, *Phase noise in oscillators: A unifying theory and numerical methods for characterization*, IEEE Trans. Circuits Systems I, 47 (2000), pp. 655–674.
- [6] F. X. KAERTNER, *Analysis of white and $f^{-\alpha}$ noise in oscillators*, Int. J. Circuit Theory Appl., 18 (1990), pp. 485–519.
- [7] G. J. CORAM, *A simple 2-D oscillator to determine the correct decomposition of perturbations into amplitude and phase noise*, IEEE Trans. Circuits Systems I, 48 (2001), pp. 896–898.
- [8] W. VANCE AND J. ROSS, *Fluctuations near limit cycles in chemical reaction systems*, J. Chem. Phys., 105 (1996), pp. 479–487.
- [9] A. HAJIMIRI AND T. H. LEE, *A general theory of phase noise in electrical oscillators*, IEEE J. Solid-State Circuits, 33 (1998), pp. 179–194.
- [10] C. H. HENRY, *Theory of the linewidth of semiconductor lasers*, IEEE J. Quantum Elec., QE18 (1982), pp. 259–264.
- [11] F. BARAS, M. M. MANSOUR, AND C. VAN DEN BROECK, *Asymptotic properties of coupled nonlinear Langevin equations in the limit of weak noise. II: Transition to a limit cycle*, J. Statist. Phys., 28 (1982), pp. 577–587.
- [12] F. BARAS AND M. M. MANSOUR, *Microscopic simulations of chemical instabilities*, Adv. Chem. Phys., 100 (1997), pp. 393–474.
- [13] R. GRAHAM, *Hopf bifurcation with fluctuating control parameter*, Phys. Rev. A., 25 (1982), pp. 3234–3258.
- [14] K. MALLICK AND P. MARCQ, *Stability analysis of a noise-induced Hopf bifurcation*, Euro. Phys. J. B, 36 (2003), pp. 119–128.
- [15] V. ALTARES AND G. NICOLIS, *Stochastically forced Hopf bifurcation: Approximate Fokker–Planck equation in the limit of short correlation times*, Phys. Rev. A., 37 (1988), pp. 3630–3633.
- [16] J. OLARREA AND F. J. DE AL RUBIA, *Stochastic Hopf bifurcation: The effect of colored noise on the bifurcation interval*, Phys. Rev. E., 53 (1996), pp. 268–271.
- [17] A. LONGTIN, *Noise-induced transitions at a Hopf bifurcation in a 1st order delay-differential equation*, Phys. Rev. A, 44 (1991), pp. 4801–4813.
- [18] K. SEYBOLD AND H. RISKEN, *On the theory of a detuned single mode laser near threshold*, Z. Physik, 267 (1974), pp. 323–330.
- [19] C. BIROCHEAU, Z. TOFFANO, AND A. DESTREZ, *Linewidth evolution in semiconductor lasers throughout threshold*, Ann. Télécommun., 49 (1994), pp. 607–618.
- [20] P. GASPARD, *Trace formula for noisy flows*, J. Statist. Phys., 106 (2002), pp. 57–96.
- [21] M. I. DYKMAN, R. MANNELLA, P. V. E. MCCLINTOCK, S. M. SOSKIN, AND N. G. STOCKS, *Noise-induced spectral narrowing in nonlinear oscillators*, Europhys. Lett., 13 (1990), pp. 691–696.
- [22] S. N. DIXIT, P. ZOLLER, AND P. LAMBROPOULOS, *Non-Lorentzian laser line shapes and the reversed peak asymmetry in double optical resonance*, Phys. Rev. A, 21 (1980), pp. 1289–1296.
- [23] M. ABRAMOWITZ AND I. A. STEGUN, *Handbook of Mathematical Functions*, Dover, New York, 1965.
- [24] A. PIKOVSKY, M. ROSENBLUM, AND J. KURTHS, *Synchronization*, Cambridge University Press, Cambridge, UK, 2001.
- [25] S. VICIANI, M. GABRYSCH, F. MARIN, F. MONTI DI SOPRA, M. MOSER, AND K. HEINZ GULDEN, *Lineshape of a vertical cavity surface emitting laser*, Optics Commun., 206 (2002), pp. 89–97.
- [26] F. HERZEL, *An analytical model for the power spectral density of a voltage-controlled oscillator and its analogy to the laser linewidth theory*, IEEE Trans. Circuits Systems I, 45 (1998), pp. 904–908.
- [27] J. P. GLEESON, O. M. ROCHE, J. WEST, AND A. GELB, *Modelling annular micromixers*, SIAM J. Appl. Math., 64 (2004), pp. 1294–1310.
- [28] K. BAJER, A. P. BASSOM, AND A. D. GILBERT, *Accelerated diffusion in the centre of a vortex*, J. Fluid. Mech., 437 (2001), pp. 395–411.
- [29] M. P. VAN EXTER, W. A. HAMEL, J. P. WOERDMAN, AND B. R. P. ZEIJLMANS, *Spectral signature of relaxation oscillations in semiconductor lasers*, 28 (1992), pp. 1470–1478.